Effect of Boundary Scattering on Magneto-Transport Performance in BN-Encapsulated Graphene

Lijun Zhu(朱丽君)[1,2,3], Lin Li(李林)[1,2,3*], Xiaodong Fan(范晓东)[1,2,3], Zhongniu Xie(谢忠纽)[1,2,3], and Changgan Zeng(曾长淦)[1,2,3*]

[1]*CAS Key Laboratory of Strongly Coupled Quantum Matter Physics, and Department of Physics, University of Science and Technology of China, Hefei 230026, China*
[2]*International Center for Quantum Design of Functional Materials (ICQD), Hefei National Research Center for Physical Sciences at the Microscale, University of Science and Technology of China, Hefei 230026, China*
[3]*Hefei National Laboratory, University of Science and Technology of China, Hefei 230088, China*

(Received 21 June 2022; accepted manuscript online 24 August 2022)

For conductors in the ballistic regime, electron-boundary scattering at the sample edge plays a dominant role in determining the transport performance, giving rise to many intriguing phenomena like low-field negative magnetoresistance effect. We systematically investigate the magneto-transport behaviors of BN-encapsulated graphene devices with narrow channel width W, wherein the bulk mean free path $L_{\rm mfp}$ can be very large and highly tunable. By comparing the magnetoresistance features and the amplitude of $L_{\rm mfp}$ in a large parameter space of temperature and carrier density, we reveal that the boundary-scattering-dominated negative magnetoresistance effect can still survive even when the ballistic ratio ($L_{\rm mfp}/W$) is as low as 0.15. This striking value is much smaller than the expected value for achieving (quasi-) ballistic transport regime ($L_{\rm mfp}/W \geq 1$), and can be attributed to the ultra-low specularity of the sample edge of our graphene devices. These findings enrich our understanding of the effects of boundary scattering on channel transport, which is of vital importance for future designs of two-dimensional electronic devices with limited lateral sizes.

DOI: 10.1088/0256-307X/39/9/097302

In high-quality two-dimensional (2D) electronic systems, the bulk mean free path of carrier ($L_{\rm mfp} = \hbar\mu\sqrt{\pi n}/e$, where $\hbar$ is Planck's constant, μ is the carrier mobility, n is the carrier density, and e is the elementary charge) determined by inelastic scatterings from impurities and phonons can be very large, and typical (quasi-) ballistic transport behaviors will emerge when $L_{\rm mfp}$ is comparable to the sample size.[1] In such (quasi-) ballistic systems, the charge carrier has a higher scattering probability at channel boundaries than in the bulk region. When boundary scattering is diffusive, applying a magnetic field B induces bending of electron trajectories and suppresses the probability of boundary scattering of electrons, resulting in negative magnetoresistance (MR) instead of classical positive MR.[2–5]

In past years, numerous experimental and theoretical studies have revealed a number of transport features originating from the high ballisticity of the conducting channel in systems represented by semiconductor quantum wells and graphene.[2–9] Many of these features can be attributed to the modulation of electron-boundary scattering under external fields. For a narrow sample whose channel width W is smaller than its length, a high ballistic ratio of $L_{\rm mfp}/W$ (≥ 1) is widely recognized as an essential requirement for (quasi-) ballistic transport.[3,8] However, there are several studies demonstrating that characteristic boundary-scattering-induced negative MR effects can still be observed even when $L_{\rm mfp}$ is smaller than W.[4] In this study, we further explore the limiting condition for the contribution of boundary scattering to channel transport using BN-encapsulated graphene as a model system, in which a large and highly tunable $L_{\rm mfp}$ can be achieved.[6,10,11] By varying temperature and carrier density over a wide range, the transition from the typical quasi-ballistic regime to the normal diffusive one is observed. Strikingly, we find that the lower limit of the ballistic ratio for inducing typical negative MR can be as low as 0.15, which can be attributed to the ultra-low specularity of the channel edge.

Figure 1(a) shows the schematic of the BN-encapsulated single-layer graphene device (BN/SLG/BN). Mechanically exfoliated SLG flake was encapsulated by two hBN flakes via a typical van der Waals assembly technique[11] and then stacked on a SiO_2/Si substrate. After shaping the device into a hall-bar geometry (sample width $W = 2\,\mu$m) by electron-beam lithography and reactive ion etching, Cr/Pd/Au with the thicknesses of 1/7/45 nm were deposited as electrode materials by electron beam evaporation. In addition to the BN/SLG/BN devices, we fabricated control samples by transferring a bare SLG flake directly onto a SiO_2/Si substrate, which are denoted as SLG/SiO_2 [see Fig. 1(d)].

Transport measurements were performed in a ^{4}He cryostat. Figure 1(b) shows the longitudinal resistance (R_{xx}) as a function of back-gate voltage ($V_{\rm BG}$) for the BN/SLG/BN device utilizing 300-nm-thick SiO_2 as the dielectric, from which a typical ambipolar field effect is observed. The Dirac point occurs at $V_{\rm D} \sim -6$ V, indicating slight electron doping. By performing Hall measurements

*Corresponding authors. Email: lilin@ustc.edu.cn; cgzeng@ustc.edu.cn
© 2022 Chinese Physical Society and IOP Publishing Ltd

at various V_{BG}, corresponding carrier density n and mobility μ can be extracted, while the latter one was calculated by using the expression $\mu = \frac{\sigma}{ne}$ with σ being the conductivity at zero magnetic field. The results plotted in Fig. 1(c) show that the carrier mobility increases when the Fermi level is tuned towards the Dirac point, with the value ranging from 61000 $cm^2/V{\cdot}s$ to 142000 $cm^2/V{\cdot}s$. These values are comparable with those reported previously.[6,10–12] As a comparison, the fabricated SLG/SiO_2 device possesses a high level of hole doping [see Fig. 1(e)], and its mobility is almost two orders of magnitude lower than that of the BN/SLG/BN device [see Fig. 1(f)].

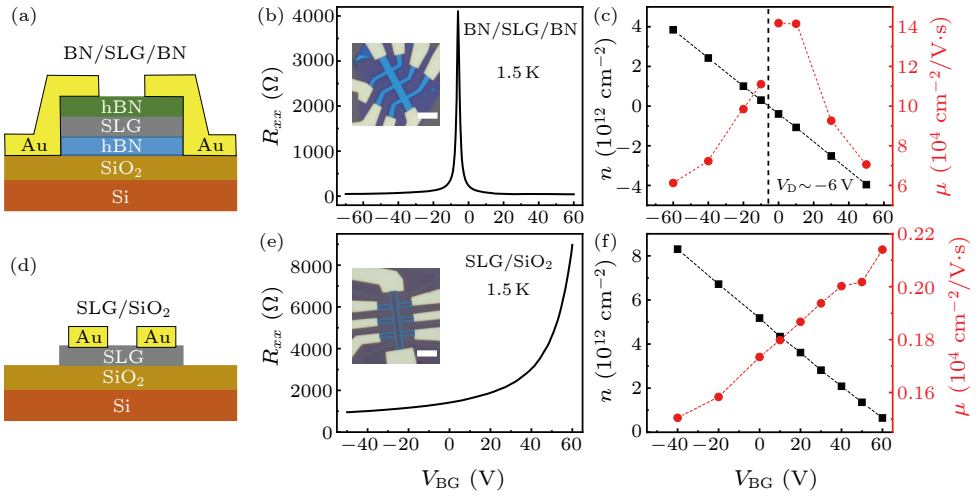

Fig. 1. Basic transport performance of the two graphene devices. [(a), (d)] Schematic illustration of the BN/SLG/BN and the SLG/SiO_2 devices, respectively. [(b), (e)] Longitudinal resistance (R_{xx}) as a function of back-gate voltage (V_{BG}) for these two devices. Insets: optical microscope images of the two devices. The scale bars are both 5 μm. [(c), (f)] Extracted carrier density and Hall mobility versus V_{BG} for the BN/SLG/BN and the SLG/SiO_2 devices, respectively. All of the measurements were made at $T = 1.5$ K.

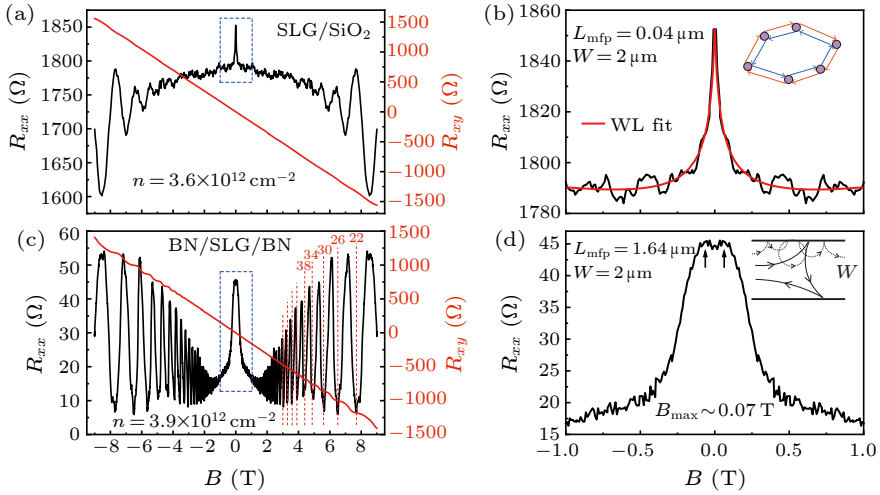

Fig. 2. Low-temperature magneto-transport behaviors: (a) R_{xx} and Hall resistance R_{xy} as functions of magnetic field B for the SLG/SiO_2 device measured at $V_{BG} = 20$ V and $T = 1.5$ K. (b) Enlarged view of R_{xx} vs B shown in (a) in the low-field regime, and the corresponding fitting result using the typical WL formula for graphene (red curve). Inset: schematic illustration of the WL effect originating from the interference between a pair of time-reversed closed loops. (c) R_{xx} and R_{xy} as functions of B for the BN/SLG/BN device measured at $V_{BG} = 50$ V and $T = 1.5$ K. Quantized Hall plateaus are clearly seen, and the corresponding filling factors are indicated. (d) Enlarged view of R_{xx} vs B shown in (c) in the low-field regime. Inset: schematic carrier trajectories in a narrow 2D channel under magnetic fields with different magnitudes.

Next, we focused on the magneto-transport performance under a perpendicular magnetic field B. Representative results for the SLG/SiO_2 device clearly show Shubnikov-de Haas (SdH) oscillations in R_{xx} [Fig. 2(a)]. However, the low carrier mobility hinders the ability to reach quantized Hall resistance (R_{xy}) plateaus. Conversely, for the BN/SLG/BN device with nearly the same carrier density [see Fig. 2(c)], well-defined quantized Hall plateaus with filling factor $\upsilon = 22, 26, 30, \ldots$, accompanied by the minima of R_{xx}, are clearly seen, which further

demonstrate its higher quality.[13,14]

Another attractive difference between the two devices is the magnetoresistance (MR) behavior in the low-field regime. For the SLG/SiO_2 device, a sharp resistance peak of R_{xx} occurs at zero field, together with a clear negative MR effect at $B < 0.1$ T [see Fig. 2(b)]. Similar results have been widely obtained in previous graphene devices and can be attributed to the weak localization (WL) effect [inset of Fig. 2(b)].[15,16] As demonstrated in Fig. 2(b), the low-field data can be well fitted using the typical WL formula for graphene[17,18] (as detailed in Section I in the Supplemental Material). The as-extracted phase coherence length L_Φ ($L_\Phi = 381$ nm) is much higher than the inter-(intra-)valley scattering length $L_i(L_*)$ ($L_i \sim L_* = 73$ nm), indicating the presence of strong elastic inter- and intra-valley scatterings.

In the BN/SLG/BN device with substantially enhanced quality, negative MR behavior is also clearly seen in the low field regime [see Fig. 2(d)]. However, as compared with that observed in the SLG/SiO_2 device, the negative MR effect here spans a dramatically wider range of B, and the magnitude (defined as $\mathrm{MR}(B) = \{[R_{xx}(B) - R_{xx}(0)]/R_{xx}(0)\} \times 100\%$) is more than one order of magnitude larger (e.g., 53% versus 3% at 0.5 T). Furthermore, it is also failed to fit the MR data by the typical WL formula for graphene,[17,18] indicating its origins other than the WL effect.

Actually, the resistance increases at first with increasing B and then is followed by the negative MR effect described above, giving rise to a side peak of resistance occurring at $B_{\max} \sim 0.07$ T. The resulting double-peak feature is strongly reminiscent of the characteristic MR behavior of quasi-ballistic transport in narrow conducting channels of a two-dimensional electron gas (2DEG), wherein scattering of electrons at channel boundaries plays an essential role.[2–5,7,8] This is possible because the bulk mean free path L_{mfp} (1.64 μm for $n = 3.9 \times 10^{12}\,\mathrm{cm}^{-2}$) is comparable to the sample width W (2 μm). In addition, the peak field of $B_{\max}$ scales with the ratio of W to the cyclotron radius r_c of carriers as $\alpha = \frac{W}{r_c} = \frac{WeB_{\max}}{\hbar\sqrt{\pi n}} \backsim 0.6$, consistent with quasi-ballistic transport performance in semiconductor 2DEG and graphene systems.[2,4,5,7]

The low-field MR behavior of the BN/SLG/BN device can be better interpreted using the framework of quasi-ballistic transport.[2,3,8] At smaller B, the carrier cyclotron orbit induced by the Lorentz force is much larger than the sample width, i.e., $r_c = \frac{\hbar}{eB}\sqrt{\pi n} > W$. In this scenario, diffusive scattering between the channel boundaries gives rise to an increase in the backscattering probability of carriers [solid lines in the inset of Fig. 2(d)] and thus higher resistance. A higher B leads to a smaller cyclotron radius r_c, which, on the contrary, decreases the probability of electron-boundary scattering and results in a decrease in resistance. This trend with increasing B slows down when $2r_c$ is smaller than W because the carriers scattered by one boundary cannot reach the other unless they are scattered within the bulk [dashed lines in the inset of Fig. 2(d)].

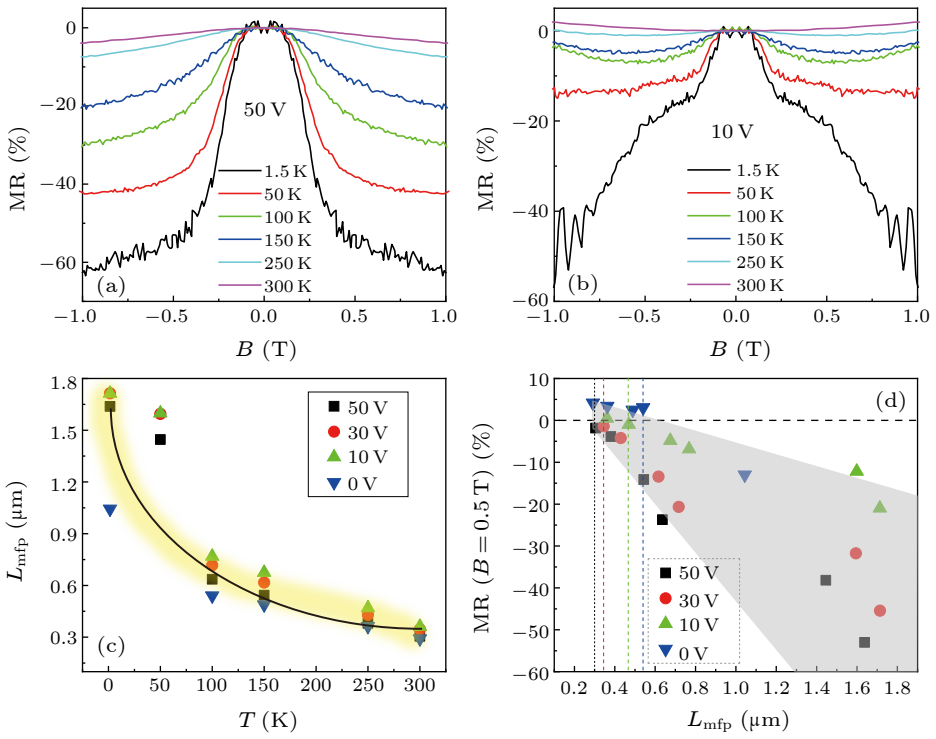

Fig. 3. Lower-limit of the bulk mean free path for inducing boundary-scattering-dominated negative MR effect in the BN/SLG/BN device. [(a), (b)] MR curves measured at different temperatures for $V_{\mathrm{BG}} = 50$ V and $V_{\mathrm{BG}} = 10$ V, respectively. (c) Extracted values of L_{mfp} under different V_{BG} as a function of temperature. The black line serves as a guide to the eyes. (d) Relation between the MR value at $B = 0.5$ T and the extracted L_{mfp}. Corresponding data were obtained from the electron side at various V_{BG} and temperatures.

Figure 3(a) presents the evolution of MR behavior across a range of temperature (for more data, see Figs. S1 and S2 in the Supplemental Material). As the temperature increases, the magnitude of negative MR decreases monotonically and the side peak at $B_{\max}$ weakens. Nevertheless, in contrast to the WL effect that normally appears at relatively low temperatures,[19–21] the boundary-scattering-dominated negative MR effect observed here is quite robust, persisting even at temperatures of up to 300 K at high doping levels ($n = 3.9 \times 10^{12}\,\mathrm{cm}^{-2}$ at $V_{\mathrm{BG}} = 50\,\mathrm{V}$). Noticeably, for low n cases with smaller negative MR at the base temperature (see Fig. 3(b) for $n = 1.1 \times 10^{12}\,\mathrm{cm}^{-2}$ at $V_{\mathrm{BG}} = 10\,\mathrm{V}$), thermally induced suppression is more evident, manifested as a classical positive MR at elevated temperatures. This temperature effect can be largely attributed to the reduction of L_{mfp} due to the enhancement of electron-phonon scattering [see Fig. 3(c)],[10,22–24] which results in a transition from quasi-ballistic to diffusive transport.

To better demonstrate the intimate relationship between L_{mfp} and the boundary scattering-dominated negative MR effect, we plot the dependence of MR (at $B = 0.5\,\mathrm{T}$) on L_{mfp} at various temperatures and gate voltages [Fig. 3(d)]. It is clear that the negative MR effect gets overall weakened with decreasing L_{mfp}, and a positive MR regime eventually emerges when L_{mfp} is smaller than a certain value [see Fig. 3(d)]. This value corresponds to the lower limit of L_{mfp}, or rather, the upper-limit of bulk scattering rate, above which boundary scattering contributes to the channel transport. Unexpectedly, this value can be as small as 0.3 μm, that is, only 0.15 times the sample width. Consistent results have also been obtained for the hole side of this BN/SLG/BN device, and another BN-encapsulated bilayer graphene device, as shown in Figs. S2 and S3 in the Supplemental Material. These results are seemingly inconsistent with previous study, since boundary scattering is taken into consideration only in the typical (quasi-) ballistic regime, when L_{mfp} is larger than W or at least comparable with it.[2,3,5,7,8]

This intriguing result may be related to the reflection properties of sample edge.[8,9] For ideal specular boundary scattering (the specularity parameter $p = 1$), carriers are elastically reflected at the edge without momentum relaxation, which results in negligible backscattering probability. However, practically there are always inevitable factors that increase the edge roughness and thus the diffusiveness of boundary scattering. Accordingly, carriers are scattered at a random angle with respect to the normal of sample edge, leading to extra backscattering. The negative MR effect described above arises from the suppression of backscattering under a magnetic field. In BN-encapsulated graphene devices, the observation of negative MR at a small ballistic ratio can thus be attributed to the ultra-low specularity of the edge, since etching graphene flakes into Hall-bar geometry will introduce dopants and defects at the edge and increase the roughness.

Note that in addition to the reduction of the negative MR magnitude, increasing temperature also leads to the broadening of the overall resistance peak. Based on previous theoretical calculations,[8] this result cannot be simply interpreted by a decrease in ballisticity. Enhanced electron-electron scatterings, with an effective scattering rate proportional to T^2,[8] play a more significant role.[25–27]

From the dashed line in Fig. 3(d), it is clear that the lower limit of L_{mfp} becomes larger as V_{BG} decreases on the electron side (i.e., the carrier density decreases). To understand this behavior, we plot the 1.5 K MR curves measured at different V_{BG} in Fig. 4(a) (see Fig. S5 for typical data for the hole side). As the carrier density decreases (indicated by the arrows), the magnitude of negative MR decreases and the side peak at $B_{\max}$ becomes less obvious, consistent with previous observations of quasi-ballistic transport.[2,3,5] For the low n case, e.g., at $V_{\mathrm{BG}} = 0\,\mathrm{V}$, the MR curve in the small field regime evolves from a double- to single-peaked structure, and typical SdH oscillation behavior occurs as the field decreases to 0.6 T.

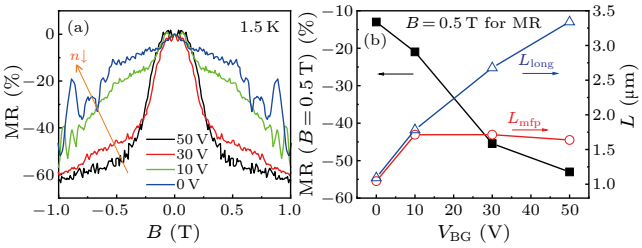

Fig. 4. Evolution of MR effect with varying V_{BG}: (a) MR curves for different V_{BG} measured at 1.5 K. (b) MR value at $B = 0.5\,\mathrm{T}$ (black line), the extracted L_{mfp} (red line) and L_{long} (blue line) as functions of V_{BG} at 1.5 K. The corresponding values of carrier density for each V_{BG} can be found in Fig. 1(c).

Based on Fig. 4(b), we find that the negative MR value at $B = 0.5\,\mathrm{T}$ (black line) is not strictly positively correlated with the extracted L_{mfp} (red line) at different V_{BG}. Although bulk mean free path is determined by various types of carrier scattering, in graphene, short-range scattering (e.g., due to neutral impurities) and long-range charged-impurity scattering are assumed to be the main contributors.[3,28] As detailed in Section Ⅱ in the Supplemental Material, the mean free path for long-range scattering (L_{long}) and for short-range scattering (L_{short}) can be extracted. L_{long} is smaller than L_{short} across a wider range of V_{BG} [see Fig. S4(c)], demonstrating the dominant role of charged-impurity scattering within the bulk region. As shown in Fig. 4(b), the amplitude of negative MR increases monotonically with increasing L_{long} at different V_{BG}, indicating that the boundary scattering effect is more pronounced when charged-impurity scattering in the bulk region get reduced, while the latter one is induced by the increasing screening effect in the cases with higher doping. This may explain why the lower limit of the ballistic ratio varies under different gate voltages.

In summary, using high-quality BN-encapsulated graphene as a model system, we have systemically investigated the evolutions of quasi-ballistic transport behaviors of a 2D conductor over a large parameter space of temperature and carrier density. We find that the typical negative MR effect dominated by electron-boundary scattering occurs even when the ballistic ratio is as low as 0.15, which can be attributed to the ultra-low specularity of the sample

edge. These findings lead us to a deeper understanding of the role of boundary scattering in transport performance of mesoscopic systems. Further optimizing the negative MR effect with high temperature robustness may have important applications in 2D electronic devices.

Acknowledgments. This work was supported by the National Natural Science Foundation of China (Grant Nos. 92165201 and 11974324), the Innovation Program for Quantum Science and Technology (Grant No. 2021ZD0302800), the Strategic Priority Research Program of Chinese Academy of Sciences (Grant No. XDC07010000), the Anhui Initiative in Quantum Information Technologies (Grant No. AHY170000), the Hefei Science Center CAS (Grant No. 2020HSC-UE014), and the Fundamental Research Funds for the Central Universities (Grant No. WK3510000013).

References

[1] Beenakker C and van Houten H 1991 *Solid State Physics* (Amsterdam: Elsevier) vol 44 chap 2 p 26
[2] Thornton T J, Roukes M L, Scherer A, and Van de Gaag B P 1989 *Phys. Rev. Lett.* **63** 2128
[3] Masubuchi S, Iguchi K, Yamaguchi T, Onuki M, Arai M, Watanabe K, Taniguchi T, and Machida T 2012 *Phys. Rev. Lett.* **109** 036601
[4] Moll P J W, Kushwaha P, Nandi N, Schmidt B, and Mackenzie A P 2016 *Science* **351** 1061
[5] Sulpizio J A, Ella1 L, Rozen A, Birkbeck J, Perello D J, Dutta D, Ben-Shalom M, Taniguchi T, Watanabe K, Holder T, Queiroz R, Principi A, Stern A, Scaffidi T, Geim A K, and Ilani S 2019 *Nature* **576** 75
[6] Mayorov A S, Gorbachev R V, Morozov S V, Britnell L, Jalil R, Ponomarenko L A, Blake P, Novoselov K S, Watanabe K, Taniguchi T, and Geim A K 2011 *Nano Lett.* **11** 2396
[7] Völkl T, Rockinger T, Drienovsky M, Watanabe K, Taniguchi T, Weiss D, and Eroms J 2017 *Phys. Rev. B* **96** 125405
[8] Raichev O E, Gusev G M, Levin A D, and Bakarov A K 2020 *Phys. Rev. B* **101** 235314
[9] Uredat P, Kodaira R, Horiguchi R, Hara S, Beyer A, Volz K, Klar P J, and Elm M T 2020 *Nano Lett.* **20** 618
[10] Dean C R, Young A F, Meric I, Lee C, Wang L, Sorgenfrei1 S, Watanabe K, Taniguchi T, Kim P, Shepard K L, and Hone J 2010 *Nat. Nanotechnol.* **5** 722
[11] Wang L, Meric I, Huang P Y, Gao Q, Gao Y, Tran H, Taniguchi T, Watanabe K, Campos L M, Muller D A, Guo J, Kim P, Hone J, Shepard K L, and Dean C R 2013 *Science* **342** 614
[12] Taychatanapat T, Watanabe K, Taniguchi T, and Jarillo-Herrero P 2013 *Nat. Phys.* **9** 225
[13] Zhang Y, Tan Y W, Stormer H L, and Kim P 2005 *Nature* **438** 201
[14] Novoselov K S, Geim1 A K, Morozov S V, Jiang D, Katsnelson M I, Grigorieva I V, Dubonos S V, and Firsov A A 2005 *Nature* **438** 197
[15] Ki D K, Jeong D, Choi J H, Lee H J, and Park K S 2008 *Phys. Rev. B* **78** 125409
[16] Tikhonenko F V, Horsell D W, Gorbachev R V, and Savchenko A K 2008 *Phys. Rev. Lett.* **100** 056802
[17] McCann E, Kechedzhi K, Fal'ko V I, Suzuura H, Ando T, and Altshuler B L 2006 *Phys. Rev. Lett.* **97** 146805
[18] Wu X, Li X, Song Z, Berger C, and de Heer W A 2007 *Phys. Rev. Lett.* **98** 136801
[19] Engels S, Terrés B, Epping A, Khodkov T, Watanabe K, Taniguchi T, Beschoten B, and Stampfer C 2014 *Phys. Rev. Lett.* **113** 126801
[20] Jafarpisheh S, Cummings A W, Watanabe K, Taniguchi T, Beschoten B, and Stampfer C 2018 *Phys. Rev. B* **98** 241402
[21] Iwasaki T, Moriyama S, Ahmad N F, Komatsu K, Watanabe K, Taniguchi T, Wakayama Y, Hashim A M, Morita Y, and Nakaharai S 2021 *Sci. Rep.* **11** 18845
[22] Chen J H, Jang C, Xiao S, Ishigami M, and Fuhrer M S 2008 *Nat. Nanotechnol.* **3** 206
[23] Hwang E H and Sarma S D 2008 *Phys. Rev. B* **77** 115449
[24] Morozov S V, Novoselov K S, Katsnelson M I, Schedin F, Elias D C, Jaszczak J A, and Geim A K 2008 *Phys. Rev. Lett.* **100** 016602
[25] Alekseev P S 2016 *Phys. Rev. Lett.* **117** 166601
[26] Scaffidi T, Nandi N, Schmidt B, Mackenzie A P, and Moore J E 2017 *Phys. Rev. Lett.* **118** 226601
[27] Holder T, Queiroz R, Scaffidi T, Silberstein N, Rozen A, Sulpizio J A, Ella L, Ilani S, and Stern A 2019 *Phys. Rev. B* **100** 245305
[28] Sarma S D, Adam S, Hwang E H, and Rossi E 2011 *Rev. Mod. Phys.* **83** 407

Supplemental Material: Effect of Boundary Scattering on Magneto-Transport Performance in BN-Encapsulated Graphene

Lijun Zhu(朱丽君)[1,2,3], Lin Li(李林)[1,2,3**], Xiaodong Fan(范晓东)[1,2,3],
Zhongniu Xie(谢忠纽)[1,2,3], and Changgan Zeng(曾长淦)[1,2,3**]

[1] CAS Key Laboratory of Strongly Coupled Quantum Matter Physics, and Department of Physics, University of Science and Technology of China, Hefei 230026, China

[2] International Center for Quantum Design of Functional Materials (ICQD), Hefei National Research Center for Physical Sciences at the Microscale, University of Science and Technology of China, Hefei 230026, China

[3] Hefei National Laboratory, University of Science and Technology of China, Hefei 230088, China

I. Fitting the low-field MR data for the SLG/SiO_2 device

The low-field MR data for the SLG/SiO_2 device were fit using the following formula that is widely used to describe the WL effect in graphene,[1,2]

$$\Delta\rho(\mathrm{B}) = -\frac{e^2\rho^2}{\pi h}\left[F\left(\frac{B}{B_\Phi}\right) - F\left(\frac{B}{B_\Phi + 2B_\mathrm{i}}\right) - 2F\left(\frac{B}{B_\Phi + B_\mathrm{i} + B_*}\right)\right]$$

where $F(z) = \ln z + \Psi(\frac{1}{2} + \frac{1}{z})$, $\Psi(x)$ is the digamma function, and $B_{\Phi,i,*} = \frac{\hbar}{4e}L_{\Phi,i,*}^{-2}$. L_Φ is the phase coherence length, and L_i/L_* is the inter/intra-valley scattering length. As demonstrated in Fig. 2b, the fitting is pretty good, and the typical lengths of L_Φ, L_i and L_* can be extracted accordingly.

II. Further analysis of bulk mean free path

The carrier density dependence of conductivity helps us to identify the dominant scattering sources in the present BN/SLG/BN devices.[3] We now discuss the dependence of conductivity on V_{BG} (see Fig. S4a), considering two main types of scattering events: short-range scattering and long-range charged-impurity scattering.[4] To extract the corresponding mean free path, the conductivity (σ) at different V_{BG} is fit using a formula that includes both long- and short-range scattering, $\sigma^{-1} =$

$(ne\mu_1)^{-1} + \rho_s$, where n is the carrier density, e is the elementary charge, μ_1 is the density-independent mobility from long-range charged-impurity scattering, and ρ_s is the resistivity from short-range scattering.[4-7] Typical fitting result at 1.5 K is shown in Fig.S4a (dashed line), from which μ_1 and ρ_s are obtained. Accordingly, the mean free path for long-range charged-impurity scattering ($L_{\text{long}} = \hbar\sqrt{\pi n}\mu_1 e^{-1}$) and for short-rang scattering ($L_{\text{short}} = \hbar\sqrt{\pi n^{-1}}\rho_s^{-1}e^{-2}$) at different V_{BG} can be extracted,[8] as presented in Fig. S4b. The value of L_{long} (L_{short}) increases (decreases) when the graphene sample is tuned away from the Dirac point, consistent with previous results.[4] Figures S4c,d show three types of mean free paths (L_{mfp}, L_{long} and L_{short}) as functions of V_{BG} on the electron- and hole sides, respectively. It is clear that L_{long} is smaller than L_{short} across a wider range of V_{BG}, i.e., the scattering rate $\tau_{\text{long}}^{-1} > \tau_{\text{short}}^{-1}$, demonstrating that charged-impurity scattering is the dominant scattering source within the bulk region. When the carrier density increases, the carrier screening effect is enhanced, leading to decreased charged-impurity scattering.

Supplemental figures:

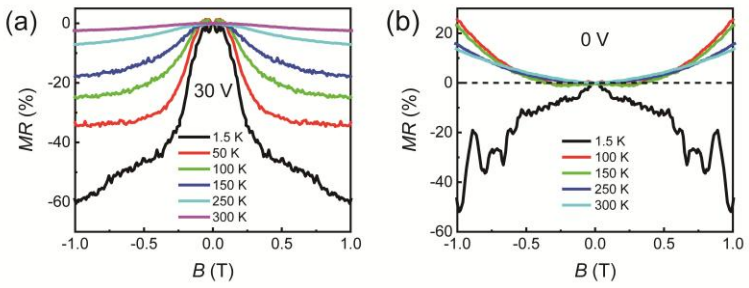

Fig. S1. MR curves measured at different temperatures for (a) V_{BG} = 30 V and (b) V_{BG} = 0 V. All data were obtained from the electron side.

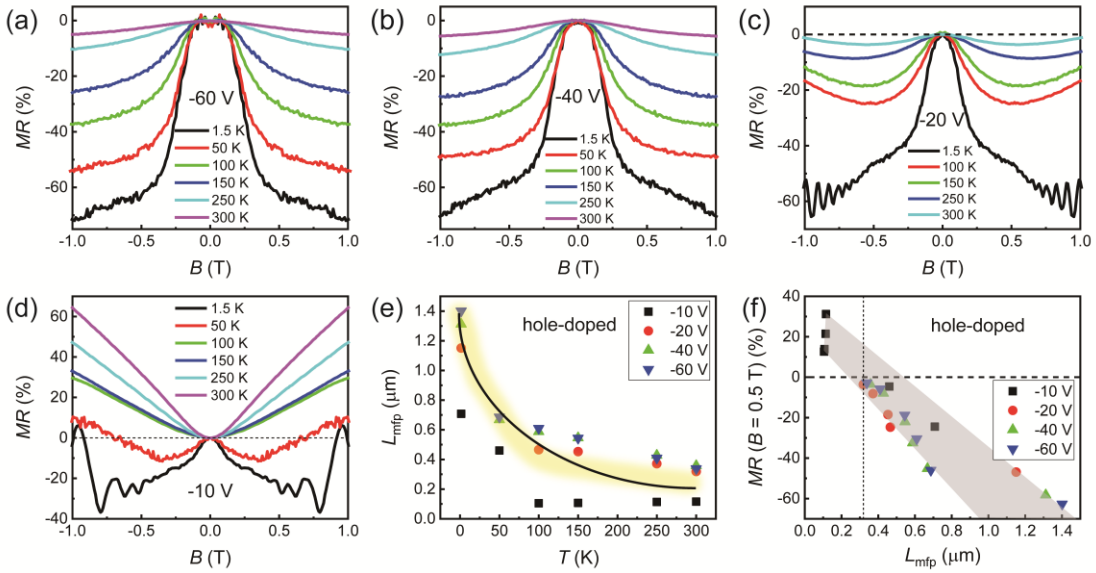

Fig. S2. Lower-limit of the bulk mean free path in the induction of boundary-scattering-dominated negative MR effect on the hole side. (a-d) MR curves measured at different temperatures for various V_{BG}: -60 V, -40 V, -20 V, -10 V. (e) Extracted values of L_{mfp} under different V_{BG} as a function of temperature. The black line serves as a guide to the eyes. (f) Relationship between the MR value at B = 0.5 T and the L_{mfp}. Corresponding data were obtained on the hole side over a range of V_{BG} and temperature. Here, the lower-limit of the ballistic ratio is 0.16 (i.e. L_{mfp}/W = 0.32 μm/2 μm), which is similar to the result obtained from the electron side (see Fig. 3d in the main text).

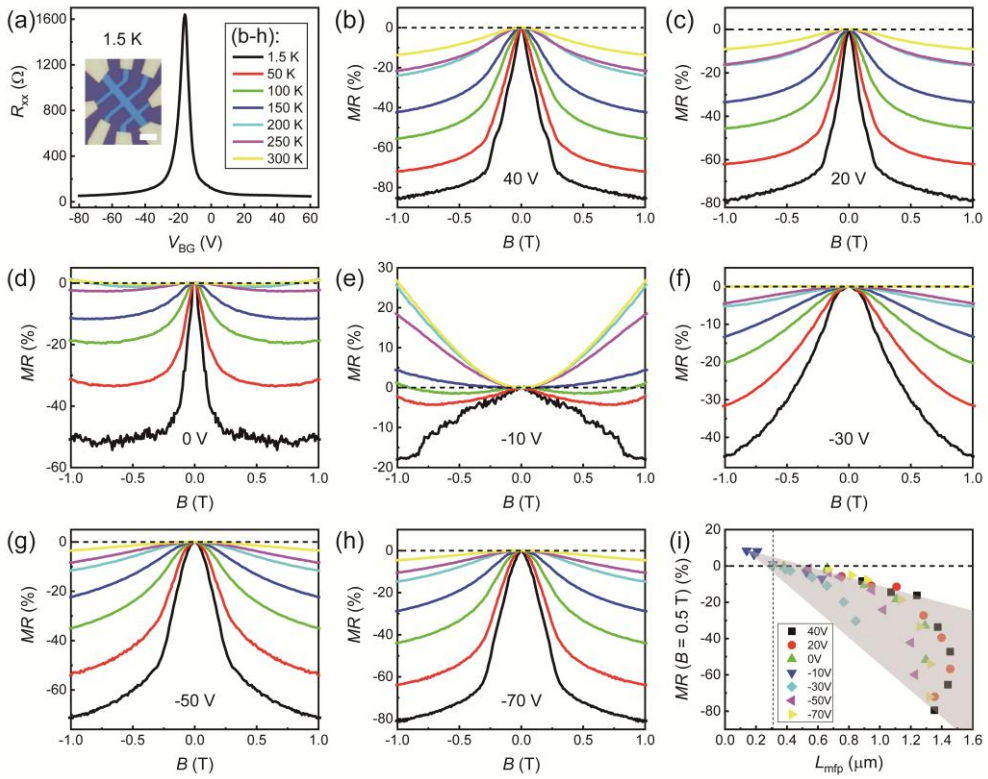

Fig. S3. Magneto-transport behaviors of a BN-encapsulated bilayer graphene device. (a) R_{xx} as a function of V_{BG} measured at 1.5 K. Inset: optical microscope image of the device. (b-h) MR curves obtained at different temperatures for various V_{BG}. (i) Relation between the MR value at B = 0.5 T and the extracted L_{mfp}. The black dashed line indicates the lower-limit of L_{mfp} for inducing boundary-scattering-dominated negative MR effect.

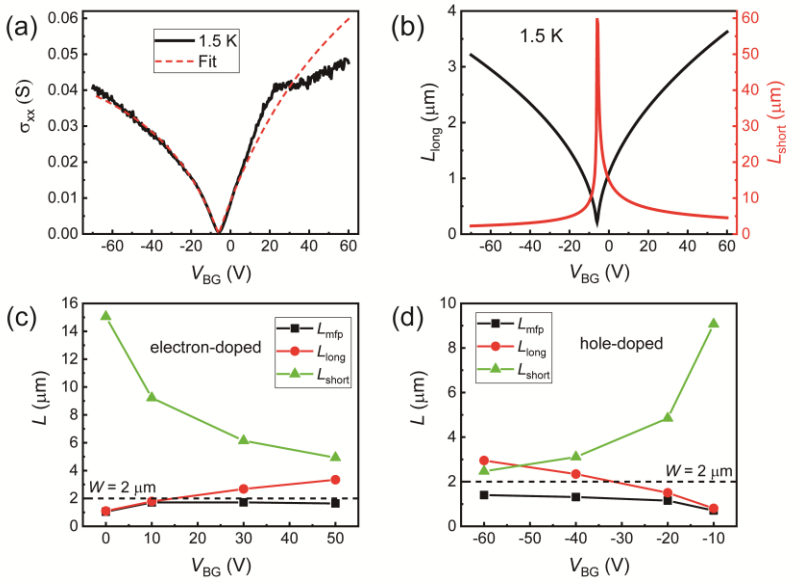

Fig. S4. Extracting L_{long} and L_{short} at different V_{BG}. (a) Conductivity (σ) as a function of V_{BG} at 1.5 K. The dashed line is fitted by the formula presented in supplementary Note 2. (b) The obtained L_{long} (black line) and L_{short} (red line) as functions of V_{BG}. (c,d) L_{mfp}, L_{long}, and L_{short} as functions of V_{BG} on the electron and hole sides, respectively.

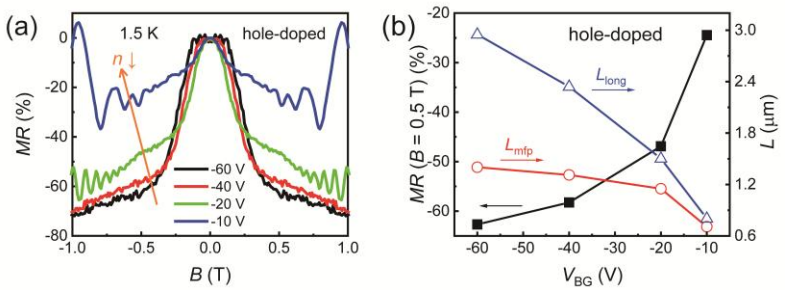

Fig. S5. Evolution of the MR effect with varying V_{BG} on the hole side. (a) MR curves for different V_{BG} measured at 1.5 K. (b) MR value at B = 0.5 T (black line) and extracted values of L_{mfp} (red line) and L_{long} (blue line) as functions of V_{BG} at 1.5 K. The corresponding values of carrier density at each value of V_{BG} can be found in Fig. 1c. It is clear that the amplitude of negative MR increases monotonically with increasing L_{long} at different V_{BG}, consistent with the results obtained from the electron side (see Fig. 4 in the main text).

Supplemental references:

[1] McCann E, Kechedzhi K, Fal'ko V I, Suzuura H, Ando T and Altshuler B L 2006 *Phys. Rev. Lett.* **97** 146805

[2] Wu X, Li X, Song Z, Berger C and de Heer W A 2007 *Phys. Rev. Lett.* **98** 136801

[3] Peres N M R 2010 *Rev. Mod. Phys.* **82** 2673

[4] Masubuchi S, Iguchi K, Yamaguchi T, Onuki M, Arai M, Watanabe K, Taniguchi T, and Machida T 2012 *Phys. Rev. Lett.* **109** 036601

[5] Nomura K and MacDonald A H 2007 *Phys. Rev. Lett.* **98** 076602

[6] Hwang E S, Adam S and Sarma S D 2007 *Phys. Rev. Lett.* **98** 186806

[7] Dean C R, Young A F, Meric I, Lee C, Wang L, Sorgenfrei1 S, Watanabe K, Taniguchi T, Kim P, Shepard K L and Hone J 2010 *Nat. Nanotechnol.* **5** 722

[8] Sarma S D, Adam S, Hwang E H and Rossi E 2011 *Rev. Mod. Phys.* **83** 407